RESEARCH PAPER

PCCP
www.rsc.org/pccp

Self-motion of a camphor disk coupled with convection

Hiroyuki Kitahata,[ab] Shin-ichi Hiromatsu,[a] Yukie Doi,[a] Satoshi Nakata*[a] and Mohammed Rafiqul Islam[c]

[a] *Department of Chemistry, Nara University of Education, Takabatake-cho, 630-8528 Nara, Japan. E-mail: nakatas@nara-edu.ac.jp; Fax: +81-742-27-9191; Tel: +81-742-27-9191*

[b] *Department of Physics, Graduate School of Science, Kyoto University, 606-8502 Kyoto, Japan*

[c] *Innovative Technology Development Division, Technical Center, U-tec Corporation, Ohmori-cho 21-1, 630-8131 Nara, Japan*

Received 2nd December 2003, Accepted 10th February 2004
First published as an Advance Article on the web 15th March 2004

The self-motion of a camphor disk on water was investigated both experimentally and theoretically. When the camphor disk moved along a one-dimensional water chamber, a convective flow was observed around the disk and the magnitude of convection decreased with an increase in the velocity of camphor motion. The camphor disk exhibited a characteristic motion that depended on the shape of the base of the chamber. The nature of the self-motion was reproduced by a numerical simulation that included the surface tension of the camphor layer as the driving force and Marangoni convection induced by the difference in surface tension around the camphor disk.

1. Introduction

Studies of self-motion under isothermal conditions may help us not only to understand chemo-mechanical energy transduction in biological systems but also to create novel artificial motors that mimic living organisms. All motor organs or organelles in living organisms work through the dissipation of chemical energy under almost isothermal and non-equilibrium conditions.[1,2] Several artificial systems that exhibit self-motion under conditions of chemical non-equilibrium have been studied under almost isothermal conditions using a gel,[3,4] liquid droplets,[5–15] or solid grains.[16]

We have been studying the self-motion of a camphor solid[17,18] or a camphor boat,[19,20] which exhibits spontaneous motion due to the difference in surface tension induced by the camphor layer development at the surface. As for the camphor boat, the difference in surface tension is made by the existence of the boat and the direction of motion is determined. In contrast, as for the camphor disk, the shape of it is symmetric and has no specific direction to move. Experimentally, the initial direction of motion is determined by the fluctuation when putting it on the water. Once it starts moving in one direction, it tends to move in the same direction because the difference in surface tension around the camphor disk is maintained during the unidirectional motion.[18] The inertia of a camphor disk also leads it to move in the same direction. We have reported that the nature of the self-motion of a camphor solid changes depending on experimental conditions (*e.g.*, scraping morphology,[17] temperature, surface tension, and the shape of the chamber[18]). Various modes of synchronized sailing of camphor boats have been observed depending on the temperature, size, and shape of the water chamber.[19,20] It has also been shown that camphor derivatives exhibit characteristic self-motion.[21,22] The essential features of this self-motion can be reproduced by a numerical simulation.[17,18,20,21] We have discussed this self-motion in terms of a difference in surface tension as the driving force. The convective flow induced by the difference in surface tension should influence the spontaneous motion, but it has not yet been considered.

In the present study, we investigated the self-motion of a camphor disk coupled with the convection around the disk. When a camphor disk moves along a one-dimensional water chamber, convection was observed around the disk and the magnitude of this convection decreased with an increase in the velocity of the camphor disk. In a further study of self-motion coupled with convection, the velocity of the camphor disk was changed depending on the depth of the chamber, which had a base shaped like saw-tooth waves. The essential features of this self-motion were reproduced by a numerical simulation that included Marangoni convection due to the surface tension of the camphor layer as the driving force.

2. Experimental section

Camphor was obtained from Wako Chemicals (Kyoto, Japan). Water was first distilled and then purified with a Millipore Milli-Q filtering system. A camphor disk (diameter: 3 mm, thickness: 1 mm) was prepared using a pellet die set for FTIR. For experiments in a one-dimensional water chamber, 3 ml of water was poured into a polystyrene chamber (inner length: 90 mm, width: 5 mm, depth: 9 mm, water level: 7 mm). A chamber with a saw-tooth-shaped base made of polycarbonate material was prepared by a fused deposition modelling process using TITAN (Stratasys Corporation) at U-tec Corporation. The temperature of the water chamber was adjusted to 293 $\pm$ 1 K with a thermoplate (TP-80, AS ONE Co. Ltd., Japan). Plastic beads (DIAION, HP20S, relative density: 1.01, Mitsubishi Chemical Co. Ltd., Japan) were mixed in the aqueous phase to visualize the convective flow around the camphor disk. The movement of the camphor disk was monitored with a digital video camera (SONY DCR-VX700, minimum time-resolution: 1/30 s) and then analysed by an image-processing system (Himawari, Library Inc., Japan).

DOI: 10.1039/b315672a

3. Results

Fig. 1 shows (a) snapshots of the self-motion of a camphor disk coupled with convection in a one-dimensional water chamber, and (b) the velocity of the camphor disk, v_{cam}. The camphor disk showed oscillatory motion along the chamber, and a wave that could be visualized with paint, a "colour wave", followed the disk with a time delay. In this case, the colour layer, which has a higher density than water, was sucked up from the bottom of the chamber to the water surface. The height of the colour wave increased and its peak caught up with the camphor disk when the camphor disk moved slowly (1 in Fig. 1). In contrast, the height decreased and its peak moved away from the camphor disk when the camphor disk moved rapidly (8 in Fig. 1).

To clarify the relationship between the magnitude of the colour wave and the velocity of the camphor motion, the camphor disk was artificially moved horizontally with a motor, as shown in Fig. 2a. The height of the colour wave, h_p, decreased, and the distance between the camphor disk and the peak of the wave, Δx_p, increased with an increase in the velocity of the camphor disk, as indicated in Fig. 2b. Here, the peak was defined as the nearest position to the camphor disk among some local maximum values.

Fig. 3a shows a streamline of the convective flow by the dispersion of plastic beads in aqueous phases with different

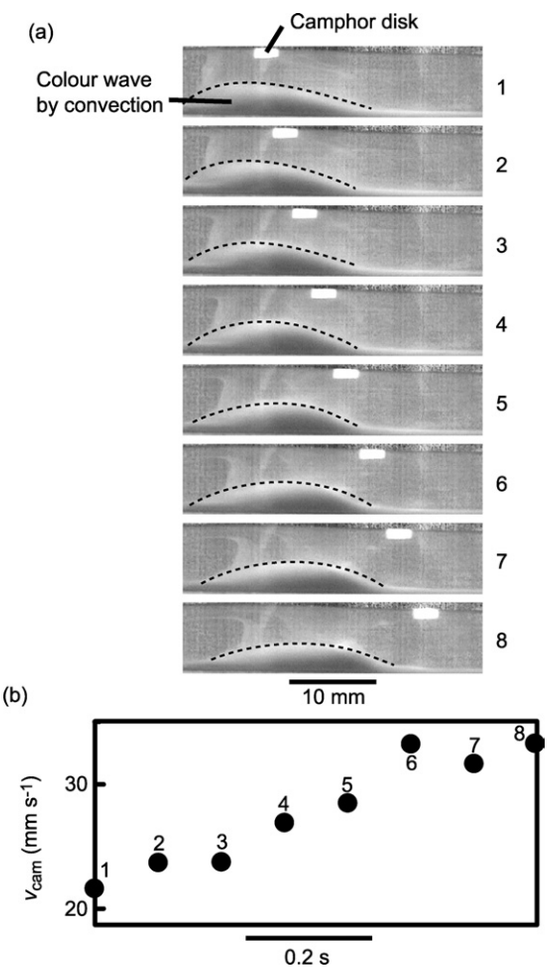

Fig. 1 (a) Snapshots of the self-motion of a camphor disk coupled with convection at a time interval of 0.1 s along the water chamber (side view). The camphor disk spontaneously moved to the right while accelerating. One ml of an aqueous paint solution (density: 1.007 g ml^{-1}) was carefully injected to the bottom of the water phase to visualize a colour wave. (b) Velocity of the camphor disk, v_{cam}. Rightward motion was defined to be positive. The numbers in (a) correspond to those in (b).

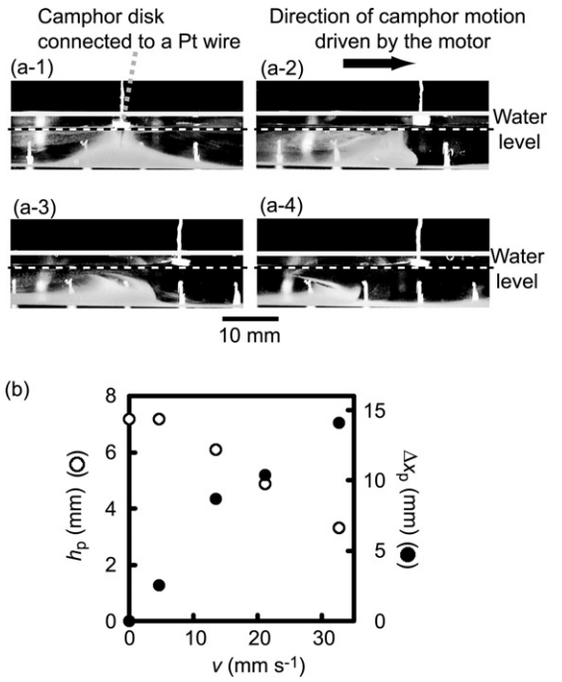

Fig. 2 (a) Snapshots of convection for camphor motion of different velocities ((1) 0, (2) 5, (3) 21, and (4) 33 mm s^{-1}) driven with a motor (side view). (b) Relationship between the velocity of the camphor motion and the nature of convection (h_p: height of the peak, Δx_p: distance between the camphor disk and the peak of the colour wave). In this experiment, a camphor disk connected to a motor *via* a platinum wire (diameter: 0.5 mm) was moved laterally with the motor.

viscosities, η_r. In this experiment, the camphor disk was fixed with a platinum wire on the water surface. The velocity of convection, v_{conv}, and the area of convection, S_{conv}, both depended on η_r, as shown in Fig. 3b-1. In this example, v_{conv} in the measured area marked in the right side of Fig. 3a was relatively high compared to that at other locations, and S_{conv} was defined as the area that experimentally showed reverse flow. v_{conv} and S_{conv} were measured from the motion of the plastic beads. They decreased with an increase in η_r. The velocity of the self-motion of a free camphor disk, v_{cam}, also depended on η_r, as shown in Fig. 3b-2. Although the surface tension remained nearly constant in this experimental condition, v_{cam} clearly decreased with an increase in η_r.

Fig. 4 shows the camphor motion on water in a chamber with a saw-tooth-shaped base. The camphor moved over three teeth under the present conditions. The maximum velocity in the leftward motion (−60 mm s^{-1}) was greater than that in the rightward motion (50 mm s^{-1}). The velocity decreased when the camphor disk passed over the edge of the saw-tooth blade while moving to the right, as marked by leftward arrows. In contrast, the velocity increased when the camphor disk passed over the edge while moving to the left, as marked by rightward arrows.

4. Discussion

4.1. Mechanism of the self-motion coupled with the convective flow

Based on the experimental results and previous papers on the self-motion of camphor,[16–18] we discuss the relationship between self-motion and convection.

Figs. 1 and 2 suggest that the camphor disk resting on the water surface can enhance the velocity of the convective flow (or the height of the colour wave) due to Marangoni convection.[23] When it rests on a water surface, while the concentration of the camphor layer around the disk is locally high,

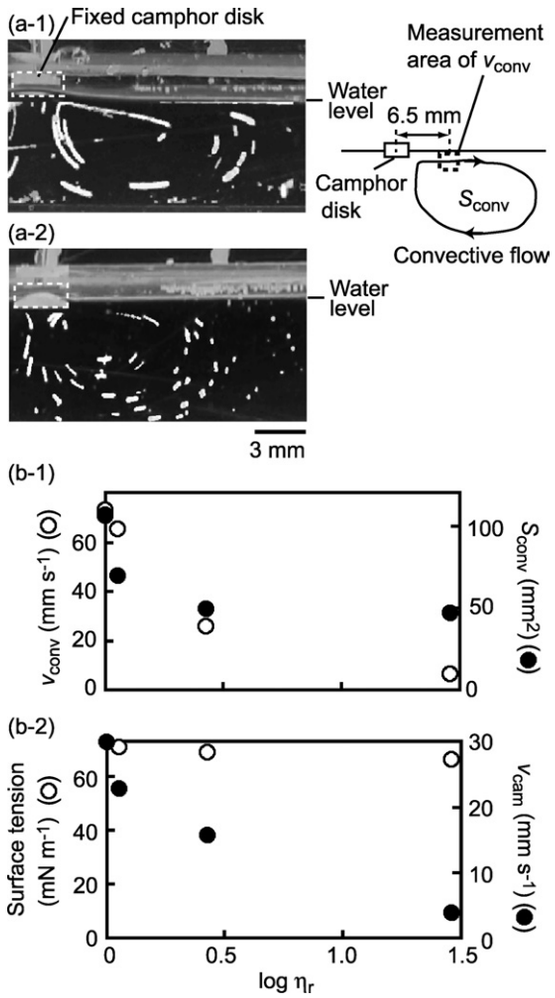

Fig. 3 (a) Trajectories of convective flow (analysed time: 1/3 s), as visualized with plastic beads (diameter: 100–200 μm) in a side view when a camphor disk was placed on (a-1) the surface of an aqueous phase with 5 mol l^{-1} glycerin and (a-2) the surface of an aqueous phase with 10 mol l^{-1} glycerin. The nature of convective flow on the left side of the camphor disk (data not shown) was similar to that on the right side. (b-1) Dependence of v_{conv} and S_{conv} on the logarithm of the relative viscosity, η_r. (b-2) Dependence of the surface tension of the aqueous phase and the velocity of a free camphor disk on the aqueous phase, v_{cam}, on the logarithm of η_r. The measured area on v_{conv} is schematically indicated in the right side of Fig. 3a.

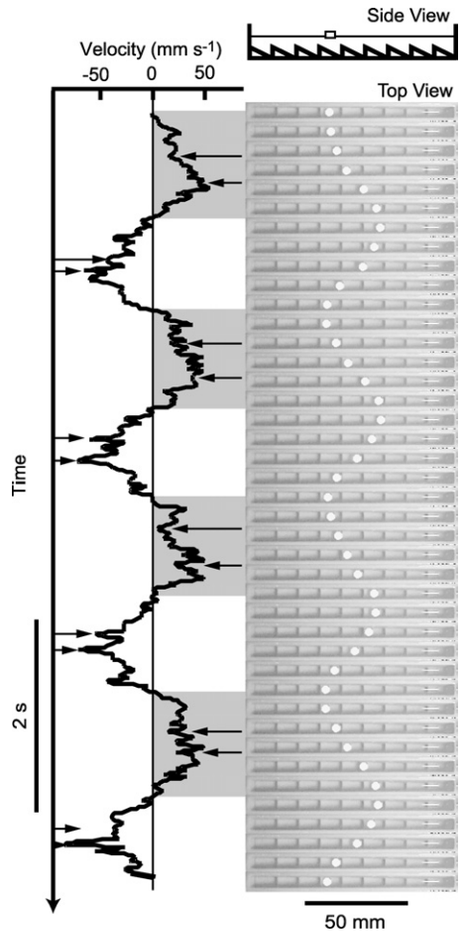

Fig. 4 Experimental result using the chamber with a saw-tooth-shaped base. Right: Snapshots of camphor motion with a time interval of 0.2 s (top view) in the chamber shown schematically (side view). Left: Time variation of the velocity of a camphor disk. The analysed data correspond to those in the snapshots on the right. The positive (grey areas) and negative velocities correspond to motion to the right and left in the chamber. The rightward and leftward arrows denote when the camphor disk passed over the front edge of a saw-tooth blade from the right to the left and *vice versa*, respectively.

the concentration at the water surface away from the disk remains low due to sublimation. Therefore, the concentration gradient of the camphor layer around the disk is very steep and convective flow (or the magnitude of the colour wave) is relatively large in the resting state, as seen in Fig. 2a-1. In contrast, the concentration gradient of the camphor layer will be diminished when the camphor disk moves rapidly on the water surface. Therefore, the convective flow (or the magnitude of the colour wave) is reduced and the peak of the colour wave cannot catch up with the self-motion of the camphor disk, as seen in Fig. 2a-4. Fig. 3 suggests that the driving force of the self-motion is reduced with an increase in viscosity even under a nearly constant surface tension, as reflected in the velocity and magnitude of convective flow.

Fig. 4 suggests that symmetric oscillatory motion along a water chamber with a flat base changes to asymmetric oscillatory motion when asymmetry is introduced to the water chamber, *i.e.*, by using a chamber with a saw-tooth-shaped base. When the camphor disk is located above the edge of a saw-tooth blade (at the minimum depth of the chamber), the magnitude of convective flow on the right side of the camphor disk is lower than on the left side due to the difference in the water level between the left and right sides. We found that the magnitude of convection increased with an increase in the depth of water (data not shown). Thus, leftward and rightward motion above the blade may be accelerated and decelerated, respectively, by asymmetric convective flow around the camphor disk. Regarding the effect of the water level, the time variation of the velocity of the camphor disk in unidirectional motion is the same as that for motion in the opposite direction when the water level in the chamber with a saw-tooth-shaped base is sufficiently high. Thus, the shape of the base strongly affects convective flow and changes the velocity of self-motion.

4.2. Numerical simulation of the self-motion due to Marangoni convection induced by a difference in surface tension

To investigate the effect of convection on self-motion, we performed numerical calculations. The Navier–Stokes equation modified with a surface tension term was adopted in this report.[23–27] The incompressibility of the medium (water) is described as:

$$\vec{\nabla} \cdot \vec{v} = 0. \quad (1)$$

The modified Navier–Stokes equation is written as:[25,26,28]

$$\rho\left(\frac{\partial}{\partial t} + \vec{v} \cdot \vec{\nabla}\right)\vec{v} = \eta\nabla^2\vec{v} - \vec{\nabla}p + \vec{F}_S, \quad (2)$$

where ρ is the density of the medium, $\vec{v}$ is the fluid velocity, η is the viscosity of the medium, and p is the pressure. $\vec{F}_S$ is the surface tension, which is not zero only near the surface. In this study, it is introduced as a volume force,

$$\vec{F}_S = \begin{cases} \dfrac{\partial \gamma}{\partial x}\vec{e}_x & 0 < y < \delta, \\ 0 & y \geq \delta. \end{cases} \quad (3)$$

Here, Cartesian coordinates are set so that the surface meets the x axis, y is the depth from the water surface, $\vec{e}_x$ is the unit vector in x direction, and δ is the typical thickness of the surface. Now, the surface tension, γ, which depends on the surface concentration of the camphor layer on the water surface, c, can be approximated as:[18]

$$\gamma(c) = \frac{c_0}{c + a}, \quad (4)$$

where c_0 and a are the positive constants, and c_0/a is the surface tension at the pure water surface. On the other hand, the camphor disk forms a molecular layer on the water surface, and it sublimates to the air phase. This process is described by the reaction–diffusion equation,[21]

$$\frac{\partial c}{\partial t} + \vec{v} \cdot \vec{\nabla} c = -\alpha c + D\nabla^2 c + F(x, x_c), \quad (5)$$

where α is the rate of sublimation, D is the diffusion constant of camphor molecules on the water surface, and x_c corresponds to the position of the centre of the camphor disk. $F(x,x_c)$ corresponds to the development of camphor molecules from the camphor disk to the water surface:

$$F(x, x_c) = \begin{cases} b(\tilde{c} - c) & \text{if} |x - x_c| < r, \\ 0 & \text{otherwise}, \end{cases} \quad (6)$$

where b is the rate of deliquescence from the camphor, $\tilde{c}$ is the saturated surface concentration of the camphor layer, and r is the radius of the camphor disk.

We should be able to calculate self-motion by using the following Newtonian equation, as in a previous report on the motion of the camphor:[18]

$$m\frac{d^2 x_c}{dt^2} = -k\left(\frac{dx_c}{dt} - \vec{v} \cdot \vec{e}_x\right) + 2r(\gamma(x_c + r) - \gamma(x_c - r)), \quad (7)$$

where k is the constant of resistance on the surface, and m is the mass of the camphor disk. In this report, however, we do not calculate the movement of the camphor disk for simplicity.

In the above formulations, the parameters ρ, η, c_0/a, α, D, and r can be decided by the experiments or references. However, δ, a, b, and $\tilde{c}$ are the parameters which we cannot know directly from the observation, so we selected them to qualitatively reproduce the experimental results. Therefore, we can discuss the numerical results only in a qualitative manner.

Using eqns. (1)–(6), we performed numerical calculations. First, when a camphor disk was fixed at the origin, the profile of fluid velocity was calculated. We used the slip boundary condition at the surface and the fixed boundary condition at the sides and base of the chamber. As for the concentration of the camphor layer, we used the Neumann boundary condition. Together with the development of a camphor layer on the water surface, Marangoni convection can be seen, and the outward flow along the water surface is rapid, as shown in Fig. 5. This profile of the convection is qualitatively similar to the experimental results shown in Fig. 3a.

Next, we considered a system in which the camphor disk moves at a constant velocity. Fig. 6 shows the maximum upward flow velocity and the horizontal distance between the point at which the camphor disk exists and the point at which upward flow velocity is a maximum. When the velocity of the camphor is low, the induced convective flow is large, and *vice versa*. There are qualitative correspondences between the numerical and experimental results, as shown in Fig. 2.

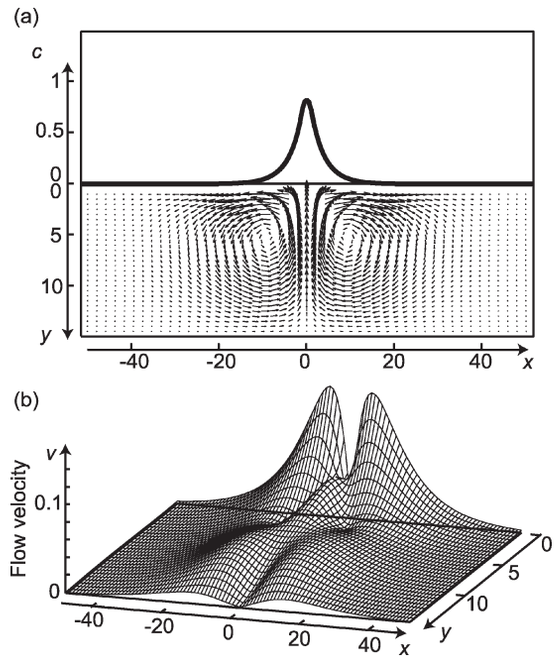

Fig. 5 Results of the numerical calculation. It is assumed that a camphor disk is fixed at the origin. (a) The surface concentration of the camphor layer and the flow velocity at representative points are shown. (b) To clarify the magnitude of the flow velocity, the absolute value of the flow velocity is shown. These profiles are qualitatively similar to those in the experimental results shown in Fig. 3a. The parameters used here are $\rho = 1.0$, $\eta = 1.0$, $c_0 = 1.0$, $a = 1.0$, $r = 1.0$, $\alpha = 0.1$, $D = 0.5$, $b = 1.0$, and $\tilde{c} = 1.0$.

The numerical results regarding the viscosity of the medium are shown in Fig. 7. As the viscosity increases, the flow velocity of the convection decreases, and the range in which convective flow is generated becomes narrower. These results qualitatively correspond to the experimental findings shown in Fig. 3.

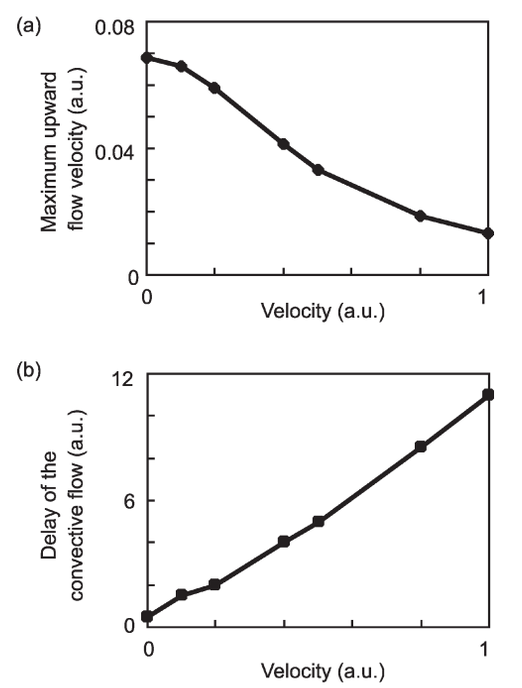

Fig. 6 Results of the numerical calculation when the camphor disk is moved at a constant velocity. (a) The maximum upward flow velocity and (b) the horizontal distance between the point at which the camphor disk exists and the point at which the upward flow velocity is a maximum are plotted depending on the velocity of the camphor disk. These results are similar to the experimental findings shown in Fig. 2. The parameters are the same as those used in Fig. 5.

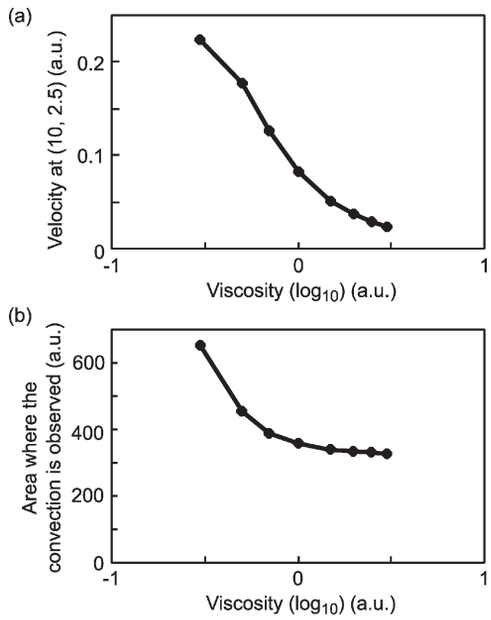

Fig. 7 The numerical results as a function of viscosity. (a) The maximum velocity and (b) the area where convective flow can be observed are plotted depending on the logarithm of the viscosity. The area is defined as where the velocity potential is more than one-tenth of the maximum value. These results are qualitatively similar to the experimental findings shown in Fig. 3. The parameters, except for the viscosity, η, are the same as those used in Fig. 5.

Fig. 8 shows the results of a numerical calculation under a saw-tooth-shaped boundary condition. Leftward flow is stronger than rightward flow near the camphor disk ($x = 0$). Due to this stronger leftward flow, leftward motion of the camphor disk is accelerated and the rightward motion is decelerated near the edges of the saw-tooth blades. The experimental results shown in Fig. 4 can be explained by this influence of the asymmetric boundary condition.

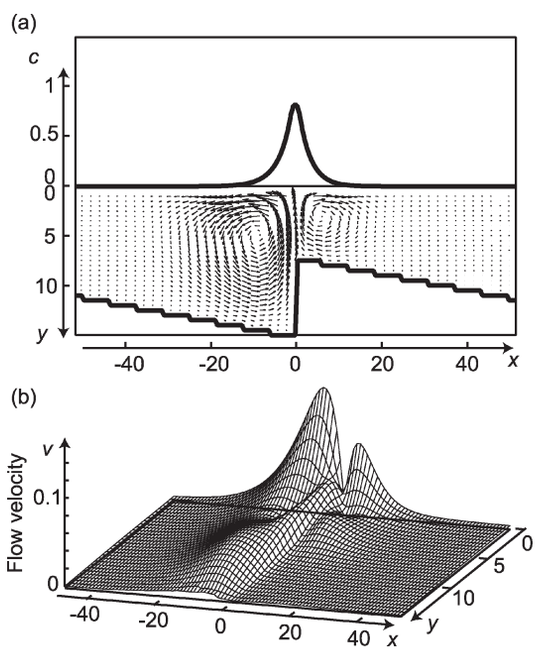

Fig. 8 The numerical results under a saw-tooth-shaped boundary condition. (a) The surface concentration of the camphor layer and the flow velocity at the representative points are shown. (b) To clarify the magnitude of the flow velocity, the absolute value of the flow velocity is shown. Leftward flow is stronger than rightward flow near the camphor disk. Due to this stronger leftward flow, leftward motion of the camphor disk is accelerated and rightward motion is decelerated near the edges of the saw-tooth blades. The experimental trends shown in Fig. 4 can be explained by this influence of the asymmetry in the boundary condition. The parameters are the same as those used in Fig. 5.

5. Conclusion

We examined the self-motion of a camphor disk in relation to the development of a camphor layer around the disk. Results showed that the self-motion depended on the surface tension, and Marangoni convection. The Marangoni convection evolves from the difference in surface tension, which works as the driving force for the camphor motion. A theoretical simulation qualitatively reproduced the experimental results. In experiments with an asymmetric chamber, convective flow changed the velocity of self-motion as a function of the depth of the water, and a similar result was seen in the simulation. In this experiment, the nature of self-motion changed due to anisotropy of the base of the chamber. Our results suggest that we should be able to induce various types of self-motion that depend on the nature of the camphor derivative and change their vector and mode by introducing anisotropic conditions to the reaction field.[29–31]

Acknowledgements

We thank Professor Masaharu Nagayama (Kyoto University, Japan) for his helpful discussions regarding the mechanism of self-motion. This study was supported by a Grant-in-Aid for Scientific Research from the Ministry of Education, Culture, Sports, Science and Technology of Japan (No. 14540559) to S. N., and a Grant-in-Aid for JSPS fellows from the Ministry of Education, Culture, Sports, Science and Technology of Japan (No. 5490) to H. K.

References

1 E. Schrödinger, *What is life?*, Cambridge University Press, Cambridge, 1944.
2 K. Yoshikawa and H. Noguchi, *Chem. Phys. Lett.*, 1999, **133**, 10.
3 R. Yoshida, T. Takahashi, T. Yamaguchi and H. Ichijo, *J. Am. Chem. Soc.*, 1996, **118**, 5134.
4 R. Yoshida, M. Tanaka, S. Onodera, T. Yamaguchi and E. Kokufuta, *J. Phys. Chem. A*, 2000, **104**, 7549.
5 T. Yamaguchi and T. Shinbo, *Chem. Lett.*, 1989, 935.
6 M. K. Chaudhury and G. M. Whitesides, *Science*, 1992, **256**, 1539.
7 F. Brochard, *Langmuir*, 1989, **5**, 432.
8 N. Magome and K. Yoshikawa, *J. Phys. Chem.*, 1996, **100**, 19 102.
9 L. E. Scriven and C. V. Sternling, *Nature*, 1960, **187**, 186.
10 Yu. Yu. Stoilov, *Langmuir*, 1998, **14**, 5685.
11 Yu. Yu. Stoilov, *Phys.-Uspekhi*, 2000, **43**, 39.
12 C. Bain, G. Burnett-Hall and R. Montgomerie, *Nature*, 1994, **372**, 414.
13 F. Domingues dos Santos and T. Ondarçuhu, *Phys. Rev. Lett.*, 1995, **75**, 2972.
14 S. Nakata, H. Komoto, K. Hayashi and M. Menzinger, *J. Phys. Chem. B*, 2000, **104**, 3589.
15 P. G. de Gennes, *Physica A (Amsterdam)*, 1998, **249**, 196.
16 L. Rayleigh, *Proc. R. Soc. London*, 1890, **47**, 364.
17 S. Nakata, Y. Iguchi, S. Ose, M. Kuboyama, T. Ishii and K. Yoshikawa, *Langmuir*, 1997, **13**, 4454.
18 Y. Hayashima, M. Nagayama and S. Nakata, *J. Phys. Chem. B*, 2001, **105**, 5353.
19 S. Nakata, M. I. Kohira and Y. Hayashima, *Chem. Phys. Lett.*, 2000, **322**, 419.
20 M. I. Kohira, Y. Hayashima, M. Nagayama and S. Nakata, *Langmuir*, 2001, **17**, 7124.
21 Y. Hayashima, M. Nagayama, Y. Doi, S. Nakata, M. Kimura and M. Iida, *Phys. Chem. Chem. Phys.*, 2002, **4**, 1386.
22 S. Nakata, Y. Doi and Y. Hayashima, *J. Phys. Chem. B*, 2002, **106**, 11 681.

23 H. Linde, P. Schwartz and H. Wilke, in *Dynamics and Instability of Fluid Interfaces*, ed. T. S. Sørensen, Springer-Verlag, 1979.
24 T. Sakurai, E. Yokoyama and H. Miike, *Phys. Rev. E: Stat. Phys., Plasmas, Fluids, Relat. Interdiscip. Top.*, 1997, **56**, 2367.
25 H. Kitahata, R. Aihara, N. Magome and K. Yoshikawa, *J. Chem. Phys.*, 2002, **116**, 5666.
26 V. I. Kovalchuk, H. Kamusewitz, D. Volhardt and N. M. Kovalchuk, *Phys. Rev. E: Stat. Phys., Plasmas, Fluids, Relat. Interdiscip. Top.*, 1999, **60**, 2029.
27 V. G. Levich, *Physicochemical Hydrodynamics*, ed. D. B. Spalding, Advance Publication, London, 1977.
28 L. D. Landau and E. M. Lifshits, *Fluid Mechanics*, Pergamon Press, London, 2nd edn., 1987.
29 N. Boccara, *Symmetries and Broken Symmetries in Condensed Matter Physics*, IDSET, Paris, 1981.
30 A. Katchalsky and P.F. Curran, *Nonequilibrium Thermodynamics in Biophysics*, Harvard University Press, Cambridge, 1965.
31 I. Prigogine, *Introduction to Thermodynamics of Irreversible Processes*, John Wiley & Sons, New York, 2nd edn., 1961.

